Biosensors and Bioelectronics 163 (2020) 112238

Contents lists available at ScienceDirect

Biosensors and Bioelectronics

journal homepage: http://www.elsevier.com/locate/bios

An electrochemical immunosensor using gold nanoparticles-PAMAM-nanostructured screen-printed carbon electrodes for tau protein determination in plasma and brain tissues from Alzheimer patients

Claudia A. Razzino [a,b,1], Verónica Serafín [a,1], Maria Gamella [a,1], María Pedrero [a], Ana Montero-Calle [c], Rodrigo Barderas [c], Miguel Calero [d], Anderson O. Lobo [e], Paloma Yáñez-Sedeño [a], Susana Campuzano [a,*], José M. Pingarrón [a,**]

[a] Department of Analytical Chemistry, Faculty of Chemical Sciences, Complutense University of Madrid, Madrid, 28040, Spain
[b] Institute of Research and Development, University of Vale do Paraiba, Sao Jose dos Campos, SP, 12244-000, Brazil
[c] Chronic Disease Programme, UFIEC, Carlos III Health Institute, Majadahonda, Madrid, 28220, Spain
[d] Alzheimer's Center Reina Sofía Foundation – CIEN Foundation and CIBERNED, Carlos III Institute of Health, Majadahonda, Madrid, 28220, Spain
[e] LIMAV – Interdisciplinary Laboratory for Advanced Materials, BioMatLab, Department of Materials Engineering, Federal University of Piaui, Teresina, PI, 64049-550, Brazil

ARTICLE INFO

Keywords:
Tau protein
Dendrimer nanocomposite
Screen-printed electrode
Amperometric sandwich immunoassay
Raw plasma
Brain tissue

ABSTRACT

This work reports a new sensitive strategy for the determination of tau protein, a hallmark of Alzheimer's disease (AD), involving a sandwich immunoassay and amperometric detection at disposable screen-printed carbon electrodes (SPCEs) modified with a gold nanoparticles-poly(amidoamine) (PAMAM) dendrimer nanocomposite (3D-Au-PAMAM) covalently immobilized onto electrografted *p*-aminobenzoic acid (*p*-ABA). The capture antibody (CAb) was immobilized by crosslinking with glutaraldehyde (GA) on the amino groups of the 3D-Au-PAMAM-*p*-ABA-SPCE, where tau protein was sandwiched with a secondary antibody labeled with horseradish peroxidase (HRP-DAb). Amperometry at −200 mV (vs the Ag pseudo-reference electrode) upon the addition of hydroquinone (HQ) as electron transfer mediator and H_2O_2 as the enzyme substrate was used to detect the immunocomplex formation. The great analytical performance of the immunosensor in terms of selectivity and low limit of detection (LOD) (1.7 pg mL^{-1}) allowed the direct determination of the target protein in raw plasma samples and in brain tissue extracts from healthy individuals and *post mortem* diagnosed AD patients, using a simple and fast protocol.

1. Introduction

According to the World Health Organization projection report, by 2040 neurodegenerative disorders (NDD) will be the second most leading cause of death worldwide, surpassing even cancer (WAR, 2015). Among NDD, one of the most frequent forms of dementia is Alzheimer's disease (AD) (Liu et al., 2013). AD causes memory loss, language deterioration, and personality changes (Ferrari et al., 2018).

From a neuropathology point of view, AD is characterized by the accumulation of two types of insoluble fibrous material: i) extracellular amyloid protein in the shape of senile plaques, with the amyloid-β (Aβ) peptide comprising 39–42 amino acids as the primary constituent of the plaques (Hardy and Higgins, 1992; Murphy and LeVine, 2010), and ii) intracellular neurofibrillary tangles (NFT) (Tolnay and Probst, 1999) consisting of accumulation of abnormal filaments composed of the microtubule-associated tau protein in a hyperphosphorylated state (Olson et al., 2005; Müller et al., 2017). Although historically, tau pathology was considered secondary to β-amyloid pathology, the accumulation of abnormal tau species is currently known to be more accurate to predict disease severity (Cook et al., 2015). Tau is a

* Corresponding author.
** Corresponding author.
E-mail addresses: susanacr@quim.ucm.es (S. Campuzano), pingarro@quim.ucm.es (J.M. Pingarrón).
[1] These authors contributed equally to this work.

https://doi.org/10.1016/j.bios.2020.112238
Received 9 January 2020; Received in revised form 14 April 2020; Accepted 23 April 2020
Available online 5 May 2020

microtubule-associated protein abundant in both the central and the peripheral nervous systems involved in microtubules assembly and stabilization. This protein participates in numerous neurological disorders grouped under the term "tauopathies", characterized by the sporadic formation of intraneuronal aggregation of the protein into neurofibrils (Tolnay and Probst, 1999; Sergeant et al., 2008), among which AD is the most prevalent (Cook et al., 2015). Recent *in vitro* studies show that full-length tau is initially present in neurons and is then mainly released as C-terminally and N-terminally truncated forms (Barthelemy et al., 2016). It has been suggested that soluble pre-filament forms of tau may be the most toxic and pathologically significant forms of tau aggregates (Lasagna-Reeves et al., 2011). Therefore, determination of tau levels holds enormous potential for early diagnosis of AD and monitoring of disease-modifying therapeutics (Müller et al., 2017).

Diagnosis of AD is complex, costly, and inaccurate, with confirmation at autopsy as the most reliable way to diagnose this disease (Wang et al., 2017). Current guidelines and recommendations for AD diagnosis intend the quantitative analysis of cerebrospinal fluid (CSF) biomarkers and use techniques such as neuropsychological testing and neuroimaging. However, many drawbacks, including invasiveness, time, cost, and accessibility to health care services, limit their widespread use as screening and diagnostic tools (Jack and Holtzman, 2013). Despite the determination of AD biomarkers has been restricted to CSF, plasma has been proposed as the ideal biofluid for their detection, since approximately 500 mL of CSF are absorbed into the blood every day (Laske et al., 2015), and it allows sample collection with minimal burden to the patients.

Tau CSF levels have been measured with enzyme-linked immunosorbent assay (ELISA) (Sparks et al., 2012; Wang et al., 2012), micro-bead based Multi-Analyte Profile (xMAP®) (Kang et al., 2012), infrared spectroscopy (Budde et al., 2019; Nabers et al., 2019), mass spectrometry (Liu et al., 2014; Barthelemy et al., 2016), surface plasmon resonance (Vestergaard et al., 2008; Kim et al., 2016) or the ultrahigh-sensitivity technology superconducting quantum interference device (SQUID) immunomagnetic reduction (IMR) assay (Chiu et al., 2013; Yang et al., 2017).

Furthermore, the low concentration of biomarkers in blood (10- to 100-fold lower than in CSF) is a challenge for accurate and reliable measurement when techniques such as ELISA are used (Blennow and Zetterberg, 2015). Big efforts have been made in the development of rapid, cost-effective, and highly sensitive methodologies using electrochemical biosensors which have proven to be useful tools to monitor protein biomarkers related to neurodegenerative disorders (Shui et al., 2018a; Hassan and Kerman, 2019; Scarano et al., 2016). It is important to mention that electrochemical affinity biosensors can detect tau in the low pM-nM level and have been applied to its determination in blood, serum, and CSF (Derkus et al., 2016, 2017; Dai et al., 2017; Wang et al., 2017; Carlin and Martic-Milne, 2018; Shui et al., 2018b; Tao et al., 2019). However, most of them require preparation times ranging between 13 and 62 h.

Integrated immuno-scaffolds implemented on disposable devices provide an interesting approach for developing electrochemical biosensors. Their analytical performance can be considerably improved by means of rational surface chemistries such as the use of diazonium salts (Moreno-Guzman et al., 2012; Conzuelo et al., 2013) and/or the coupling with smart nanomaterials (Holzinger et al., 2014; Serafín et al., 2018). Metal nanoparticles are, with no doubt, one of the most widely used nanomaterials, also as a component in the fabrication of nanocomposites, due to their unique properties including high conductivity and biocompatibility (Roduner, 2006). However, some nanosized particles have a strong tendency to agglomerate, diminishing and affecting their utility (Sauter et al., 2008). Stabilizers, also called capping agents, including polymers, surfactants and chelating agents, play an important role in the preparation of metal nanoparticles, particularly in controlling their size and preventing their aggregation in solution (Xi et al., 2012; Grillo et al., 2015). Dendrimers have been claimed as useful soft nanocontainers for the supramolecular encapsulation of nanoparticles through electrostatic or hydrophobic interactions (Sánchez et al., 2019). Among them, poly(amidoamine) (PAMAM) dendrimers are particularly useful in the synthesis of different types of metal nanoparticles such as Pt, Ag, Pd, Cu and Au (Camarada, 2017) due to their unique characteristics such as three-dimensional structure, nanometer-size (2–100 nm), low polydispersity, and high surface's functionality and flexibility (Emmrich et al., 2002). In particular, dendrimer-encapsulated metallic nanoparticles (mostly AuNPs and PtNPs) hold great promise in the fabrication of electrochemical affinity biosensors since they possess both advantages as dendrimer and the metallic nanoparticles including high density of active groups, excellent structural homogeneity, and good biocompatibility and conductivity (Zhang et al., 2016). For example, PAMAM-AuNPs and PAMAM-PtNPs nanocomposites were used as electrode modifiers (An et al., 2012; Niu et al., 2016; Singal et al., 2018) and PAMAM-AgNPs as carrier tags (Pei et al., 2013) in electrochemical immunosensors (An et al., 2012; Pei et al., 2013; Singal et al., 2018) and aptasensors (Niu et al., 2016).

Considering these antecedents, we report in this work a new integrated amperometric biosensor for the determination of tau protein. The approach involved SPCEs modified with a three-dimensional network PAMAM-AuNPs nanocomposite (3D-Au-PAMAM) as a biocompatible material and template due to the many surface functional $–NH_2$ groups. 3D-Au-PAMAM was prepared by chemical reduction of $HAuCl_4$ in the presence of G4-PAMAM, and it was covalently immobilized through carbodiimide/hydroxysulfosuccinimide (EDC/Sulfo-NHS) chemistry onto SPCEs modified with electrografted *p*-aminobenzoic acid (*p*-ABA). Unlike other related reported approaches (An et al., 2012), in this work the 3D-Au-PAMAM nanocomposite is used as scaffold to develop a sandwich immunosensor upon anti-tau capture antibody (CAb) anchoring using glutaraldehyde (GA) as cross-linking agent. A sandwich immunoassay was implemented using a detector antibody labeled with horseradish peroxidase (HRP-DAb) and amperometric detection was carried out using the H_2O_2/HQ system.

2. Materials and methods

Apparatus and electrodes, Reagents and solutions, and all the procedures used (Synthesis of 3D-Au-PAMAM, Immunosensor preparation, Electrochemical measurements and Analysis of real samples) are described in detail in the Supporting Information.

3. Results and discussion

The different steps involved in the preparation of the HRP-DAb-tau-CAb-3D-Au-PAMAM-*p*-ABA-SPCE immunosensor and the reactions implied in the amperometric transduction are shown in Fig. 1. The SPCE was functionalized by electrografting with *p*-ABA. Then, the electrode was activated via carbodiimide chemistry for the covalent immobilization of the 3D-Au-PAMAM nanocomposite through the amino groups. Subsequently, CAb was immobilized by cross-linking with GA through the interaction between the antibody amino groups and the 3D-Au-PAMAM nanocomposite. After a blocking step, the target protein was captured onto the CAb-3D-Au-PAMAM-*p*-ABA-SPCE and sandwiched with the HRP-DAb. The quantification was achieved by recording the changes in the cathodic current measured at − 0.20 V *vs.* the Ag pseudoreference electrode using the H_2O_2/HQ system (Camacho et al., 2007; Gamella et al., 2012).

The exhaustive characterization of the synthesized 3D-Au-PAMAM nanocomposite by UV–vis absorption, EDX, TEM, HRTEM and CV is discussed in detail in the Supporting Information (Figs. S1–S3).

3.1. Electrochemical monitoring of the stepwise immunosensor preparation

The successful grafting of the *p*-ABA film and the subsequent

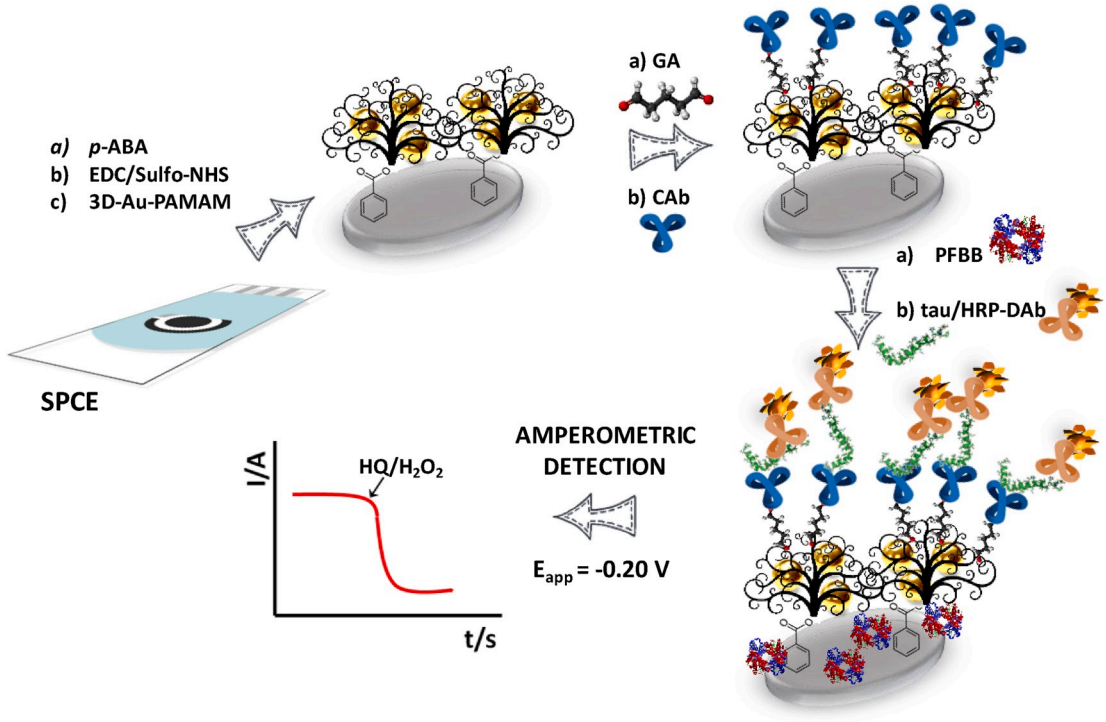

Fig. 1. Fabrication and amperometric transduction involved in the development of a HRP-DAb-tau-CAb-3D-Au-PAMAM-*p*-ABA-SPCE immunosensor for tau protein determination.

immobilization of the Au-PAMAM nanocomposite and the CAb on the HOOC-*p*-ABA-SPCE were monitored using CV and EIS in a 0.1 mol L^{-1} KCl solution containing 5 mmol L^{-1} $[Fe(CN)_6]^{3-/4-}$ as redox probe.

As expected, Fig. 2a shows a decrease in the oxidation and reduction peak currents with respect to those recorded at a bare SPCE after grafting with *p*-ABA due to the negatively charged carboxylic groups on the grafted-surface (Moreno-Guzmán et al., 2012). Moreover, the difference between the peak potentials increased from ΔE_p = 320 mV–506 mV. The increase in the peak currents observed after activation of the *p*-ABA film can be explained by the neutralization of the negative charge on the surface-confined carboxylate groups after the reaction with EDC/Sulfo-NHS (Conzuelo et al., 2012). Further bonding of 3D-Au-PAMAM gave rise to a remarkable increase in the anodic and cathodic peak currents, with $i_{pa}/i_{pc} \approx 1$, and to a decrease in the ΔE_p value down to 280 mV. This enhanced electron transfer kinetics can be attributed to the presence of AuNPs in the 3D-Au-PAMAM. The CVs overlaid in Fig. 2b display the gradual decrease of peak currents as the reagents involved in the immunosensor preparation were immobilized on the electrode surface, due to the lower conductivity provoked by the presence of insulating material.

EIS was also used to evaluate the interfacial properties of the modified electrodes. All the experimental data were obtained by fitting with a conventional Randles equivalent circuit. The corresponding Nyquist plots are displayed in Fig. 2c. In agreement with results observed by CV, an important increase in the charge transfer resistance occurred when the SPCE (R_{CT} = 729 Ω) was modified by grafting with *p*-ABA (R_{CT} = 2770 Ω), and a drastic decrease was observed after modification with 3D-Au-PAMAM (R_{CT} = 56 Ω), thus showing the benefits of the interface nanostructuring with the 3D-Au-PAMAM composite which enhance the electron transfer. In addition, as expected, successive increases in the R_{CT} value occurred upon after incubation with the CAb, blocking agents and HRP-DAb-tau mixture (R_{CT} values of 85, 141 and 154 Ω, respectively) due to the partial coating with insulating biomolecules that represent an additional barrier for the access of the redox probe to the electrode surface (Fig. 2d).

3.2. Optimization of experimental variables

Control experiments were performed with immunosensors prepared in the absence (HRP-DAb-tau-CAb-*p*-ABA-SPCEs) and in the presence of the 3D-Au-PAMAM nanocomposite (HRP-DAb-tau-CAb-3D-Au-PAMAM-*p*-ABA-SPCEs) to verify the role of the nanocomposite in the immunosensor performance and its electrocatalytic effect on H_2O_2 reduction. Fig. S4 compares the amperometric responses obtained for 0.0 and 5.0 ng mL^{-1} tau standards with the prepared immunosensors in the presence of H_2O_2/HQ and H_2O_2 (in the absence of HQ). Significantly higher amperometric responses were obtained for H_2O_2 at CAb-3D-Au-PAMAM-*p*-ABA-SPCEs compared to that obtained at CAb-*p*-ABA-SPCEs, thus demonstrating the ability of the nanomaterial to enhance the charge transfer rate. Furthermore, although a slight discrimination between the absence or the presence of tau was observed at CAb-3D-Au-PAMAM-*p*-ABA-SPCEs with no redox mediator HQ (S/B of 1.05), such discrimination was significantly improved when the electrochemical measurements were performed using the H_2O_2/HQ system (S/B of 1.9).

Optimization of other experimental variables (Fig. S5, Table S1) is discussed in detail in the Supporting Information.

3.3. Analytical characteristics

The calibration plot constructed for the amperometric detection of tau standards with the HRP-DAb-tau-CAb-3D-Au-PAMAM-*p*-ABA-SPCE immunosensor, under the optimized working conditions, is displayed in Fig. 3. A linear dependence between Δi (difference between the currents measured in the presence and in the absence of the capture antibody) (Serafín et al., 2017, 2018) vs. the logarithm of tau standard concentrations was found between 6 and 5000 pg mL^{-1} fitting to the adjusted equation Δi, nA = (776 ± 36) log [tau], ng mL^{-1} + (1973 ± 74) (r = 0.996). According to the 3 × s_b/m criterion, where s_b was estimated as the standard deviation for 20 measurements (Armbruster and Pray, 2008) carried out in the absence of tau and *m* was the slope value of the calibration plot, the calculated limit of detection was 1.7 pg mL^{-1}. The good achieved sensitivity is likely due to the combination of the large

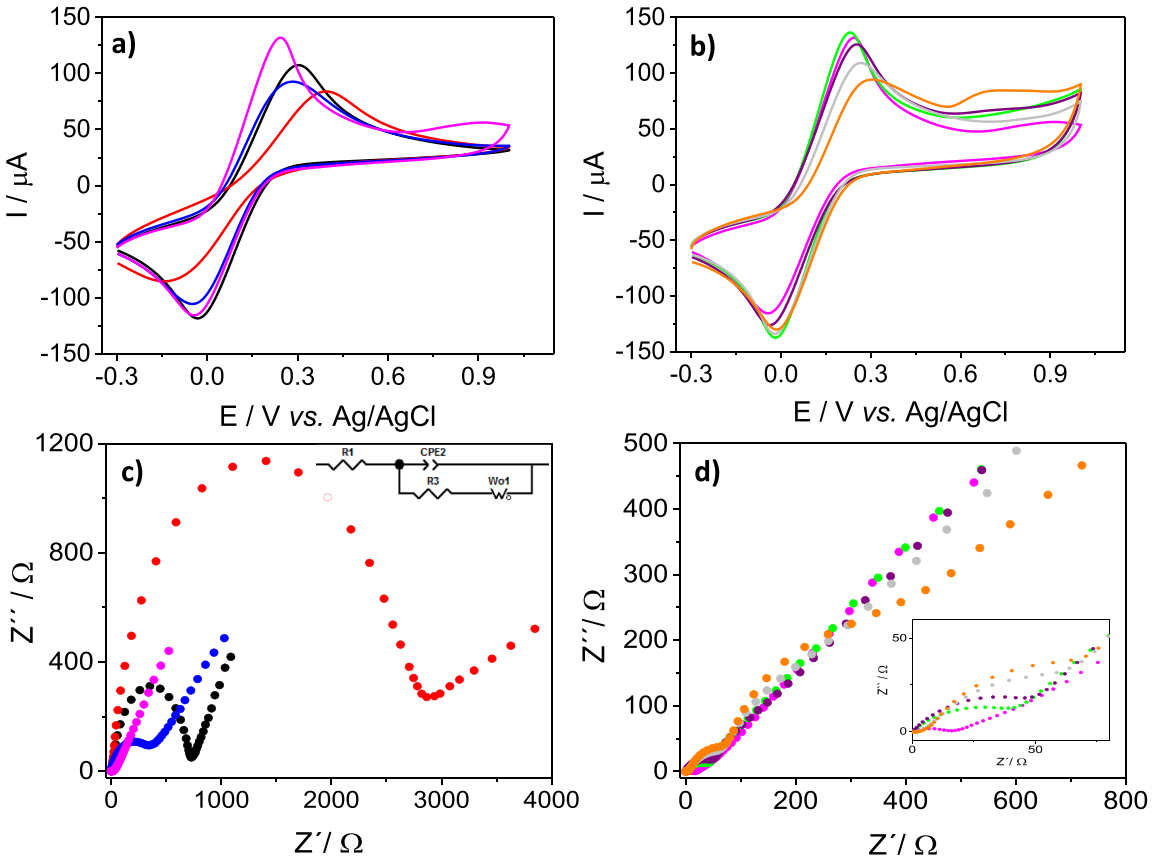

Fig. 2. (a,b) CVs and (c,d) Nyquist plots recorded in 0.1 mol L^{-1} KCl aqueous solution containing 5 mM $[Fe(CN)_6]^{3-/4-}$ at a: bare SPCE (black), HOOC-*p*-ABA-SPCE (red), EDC/Sulfo-NHS-activated HOOC-*p*-ABA-SPCE (blue), 3D-Au-PAMAM-*p*-ABA-SPCE (magenta), GA-3D-Au-PAMAM-*p*-ABA-SPCE (green), CAb-3D-Au-PAMAM-*p*-ABA-SPCE (purple), blocked CAb-3D-Au-PAMAM-*p*-ABA-SPCE (grey) and HRP-DAb-tau-CAb-3D-Au-PAMAM-*p*-ABA-SPCE (orange). CV: ν = 50 mV s^{-1}; EIS: 0.01–100,000 Hz frequency range with a 10 mV r.m.s. signal. Inset in c): equivalent circuit used to fit the experimental data. (For interpretation of the references to colour in this figure legend, the reader is referred to the Web version of this article.)

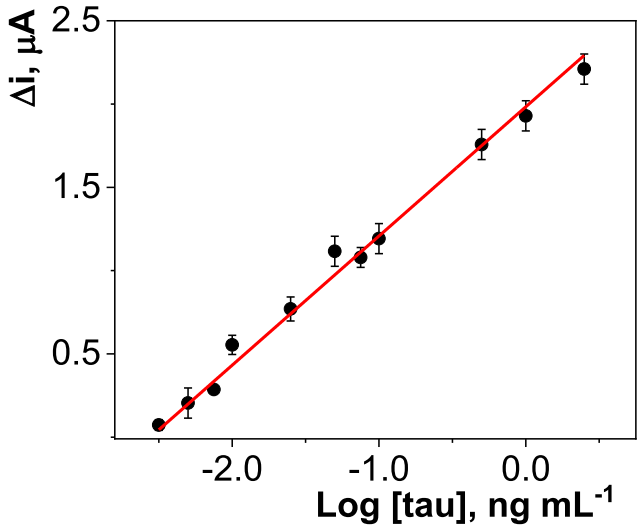

Fig. 3. Calibration plot constructed for the amperometric detection of tau standard solutions with the HRP-DAb-tau-CAb-3D-Au-PAMAM-*p*-ABA-SPCE immunosensor.

CAb loading on the 3D-Au-PAMAM-*p*-ABA-SPCEs, and the enhanced current measured at the highly conductive nanostructured electrodes (Serafín et al., 2018). It is worth mentioning that considering the established cut-off values of 450 pg mL^{-1} for a 51-70 years-old individual or 600 pg mL^{-1} for older individuals in CSF (Scarano et al., 2016), and 5 pg mL^{-1} in plasma (Blennow and Zetterberg, 2015; Müller et al., 2017), the developed immunosensor looks potentially compatible with practical applications.

The reproducibility of the responses obtained with different immunosensors was also evaluated. The comparison of the amperometric currents provided by eight different immunosensors prepared in the same manner in the same (intra-assay) or different (inter-assay) days for 0.1 ng mL^{-1} tau standard solutions, provided RSD values of 3.5 and 4.6%, respectively.

Moreover, the stability of the CAb-3D-Au-PAMAM-*p*-ABA-SPCEs (after the blocking step) was checked by storing different electrodes prepared the same day at 4 °C in a humid chamber. The as stored bioelectrodes were used as daily control to measure 0 and 2.5 ng mL^{-1} tau standard solutions. Fig. S6 in the Supporting Information shows that there were no significant differences between the S/B ratios provided by the prepared immunosensors for at least 27 days.

The analytical performance of the developed immunosensor is compared with that of previously reported electrochemical biosensors for tau protein determination (Table 1). Most of the reported methodologies require relative long and/or laborious synthesis and fabrication procedures to implement the sensing systems (up to 5 days), while the method described in this work only needs 3 h and 20 min for both to prepare the immunoplatform and perform the determination. This implies a great practical advantage versus previous immunosensors which require multiple reagents and complex and tedious substrate/nanomaterials modification protocols for signal amplification (Shui et al.,

Table 1
Main features of electrochemical affinity biosensors reported so far for the determination of tau protein.

Sensor fundamentals	Approach/Detection	Transduction technique	Analytical characteristics*	Preparation time	Sample	Ref.
AuE modified with lipoic monolayer and tau	tau–tau binding/Label-free	EIS ($Fe(CN)_6^{3-/4-}$)	L.R.: 0.2–1.0 μM	5 days	–	Esteves-Villanueva et al. (2014)
SPCE modified with GO-AlgNSp used for the immobilization of CAb	Direct immunosensor/Label-free	SFA	A.R.: 0.01-250 ng mL^{-1} (~0.18-4545 pM)	–	Blood from MS, myasthenia gravis, epilepsy, PD and healthy individuals	Derkus et al. (2016)
Thin film AuE modified with a MPA SAM and CAb	Direct immunosensor/Label-free	DPV ($Fe(CN)_6^{3-/4-}$)	L.R.: 1-100 ng mL^{-1} (~18-1818 pM)	~48 h	Human serum	Dai et al. (2017)
GO-modified SPCE and pPG dendrimers as scaffold for the immobilization anti-tau-Abs.	Sandwich immunoassay using DAb- 3.5th generation carboxyl functionalized pPG/PbS probes	DPV ($Fe(CN)_6^{3-/4-}$)	L.R.: 0.25-250 nM LOD: 150 pM	>13 h	Human serum and CSF of MS patients	Derkus et al. (2017)
Au microband electrodes covered with a DTSSP SAM, protein G and CAb	Direct immunosensor/Label-free	Tetrapolar EIS ($Fe(CN)_6^{3-/4-}$)	L.R.: 0.03-10 nM LOD: 0.03 pM	–	Spiked human serum	Wang et al. (2017)
AuE modified with a lipoic acid SAM and CAb	Direct immunosensor/Label-free	EIS ($Fe(CN)_6^{3-/4-}$)	L.R.: 1-100 μg mL^{-1} (~18-1818 nM)	62 h	–	Carlin and Martic-Milne (2018)
AuE modified with a MPA SAM and CAb	Antibody-aptamer sandwich assay using AuNPs - aptamer as amplification and detection element	DPV ($Fe(CN)_6^{3-/4-}$)	L.R.: 0.5-100 pM LOD: 0.42 pM	~45 h	Human serum	Shui et al. (2018)
GCE modified with Gr/Thi/AuNPs and a specific aptamer	Direct affinity assay	DPV (Thionin)	L.R.: 1-100 pM LOD: 0.70 pM	~16 h	Human serum	Tao et al. (2019)
SPCE modified with *p*-ABA, 3D-Au-PAMAM nanocomposite and CAb	Sandwich immunoassay using HRP-DAb	Amperometry - 0.20 V vs. Ag (HQ/H_2O_2)	L.R.: 6-5000 pg mL^{-1} (~0.11-91 pM) LOD: 0.031 pM (1.7 pg mL^{-1})	3 h 20 min	Human plasma and brain tissue extracts	This work

*The conversion between units has been done considering an average molecular weight of 55 kD for tau protein.
p-ABA: p-aminobenzoic acid; Abs: antibodies; Au: gold; A.R.: analysis range; AuE: gold electrode; AuNPs: gold nanoparticles; CAb: capture antibody; CSF: cerebrospinal fluid; DAb: detector antibody; DPV: differential pulse voltammetry; DTSSP: 3,3′-dithiobis(sulfosuccinimidyl propionate; EIS: electrochemical impedance spectroscopy; GCE: glassy carbon electrode; GO-AlgNSp: graphene oxide alginate nanosphere nanocomposite structure; Gr: graphene; HQ: hydroquinone: HRP: horseradish peroxidase; L.R.: linear range: LOD: limit of detection; MPA: mercaptopropionic acid; MS: multiple sclerosis; PAMAM: Polyamidoamine; PD: Parkinson disease; pPG: amine functionalized 1st generation trimethylolpropane tris[poly(propyleneglycol) dendrimer; SAM: self-assembled monolayer; SFA: single frequency analysis; SPCE: screen-printed carbon electrode; Thi: thionin.

2018b; Derkus et al., 2017). Moreover, only the immunosensors reported by Wang et al. (2017), Shui et al. (2018b), Tao et al. (2019) and that described in this work reach a LOD lower than the CSF tau cut-off value (4.3 pM, ~250 pg mL^{-1}) (Scarano et al., 2016). In addition, the LOD achieved with our immunosensor is very similar to the best described to date (Wang et al., 2017) which has demonstrated applicability only for spiked serum samples.

Additionally, the achieved LOD (1.7 pg mL^{-1}) is lower than those claimed for ELISA kits that range from 10 to 100 pg mL^{-1}. Furthermore, the ELISA procedures require assay times longer than 4 h, once the CAb-plate is prepared and blocked, whereas the determination of tau using the developed immunoplatform can be done in a 1-h single-step, starting since the preparation of the CAb-3D-Au-PAMAM-*p*-ABA-SPCE.

Therefore, the developed methodology is competitive both with other previously described electrochemical biosensors and with the conventional ELISA methodology in terms of sensitivity, simplicity and test time. Moreover, in comparison with ELISA, the proposed immunosensor employs affordable and portable instrumentation, which makes it a suitable tool to carry out high throughput routine tau determinations at the point of care (POC) by any laboratory. Indeed, although there is still a long way, considering that the methodology is implemented on disposable electrodes and requires only one incubation step, one could envision a future POC electrochemical device based on the proposed strategy similar to the one currently used by diabetic people to control glucose levels.

3.4. Selectivity

In order to apply the developed immunoplatform to the determination of total tau protein in clinical samples such as plasma and tissue extracts, its selectivity was tested against various potentially interfering compounds coexisting in these samples, such as human IgGs, hemoglobin, human serum albumin (HSA) and bovine serum albumin (BSA). The tests were made by measuring 0.0 and 2.5 ng mL^{-1} tau standard solutions in the absence and in the presence of the non-target proteins at the respective concentration level expected in serum of healthy individuals. As can be seen in Fig. 4a, despite the high concentrations of the potential interfering compounds, no significant effect was apparent on the determination of tau. Slightly higher signals were obtained in the presence of hemoglobin (bars 2), which is probably due to its peroxidase activity (Grigorieva et al., 2013). However, no significant difference was apparent in the S/B ratio, which makes it possible to determine tau protein in its presence.

3.5. Analysis of plasma and tissue extracts samples

The practical usefulness of the developed immunosensor was tested by determining the endogenous content of tau protein in brain tissue protein extracts and plasma samples from healthy individuals and AD patients. It is worth noting that no sample treatment was required, which is an excellent operational characteristic of the immunosensor considering these determinations are particularly challenging due to the complexity of the matrix (tissue protein extracts) and the high sensitivity required (plasma) (Blennow and Zetterberg, 2015; Müller et al., 2017). The potential existence of matrix effects was evaluated by constructing calibration plots spiking 2.5 μg of tissue extract and 5 μL of undiluted plasma with increasing concentrations of tau protein standards. Statistically significant differences were found between the slope value of the

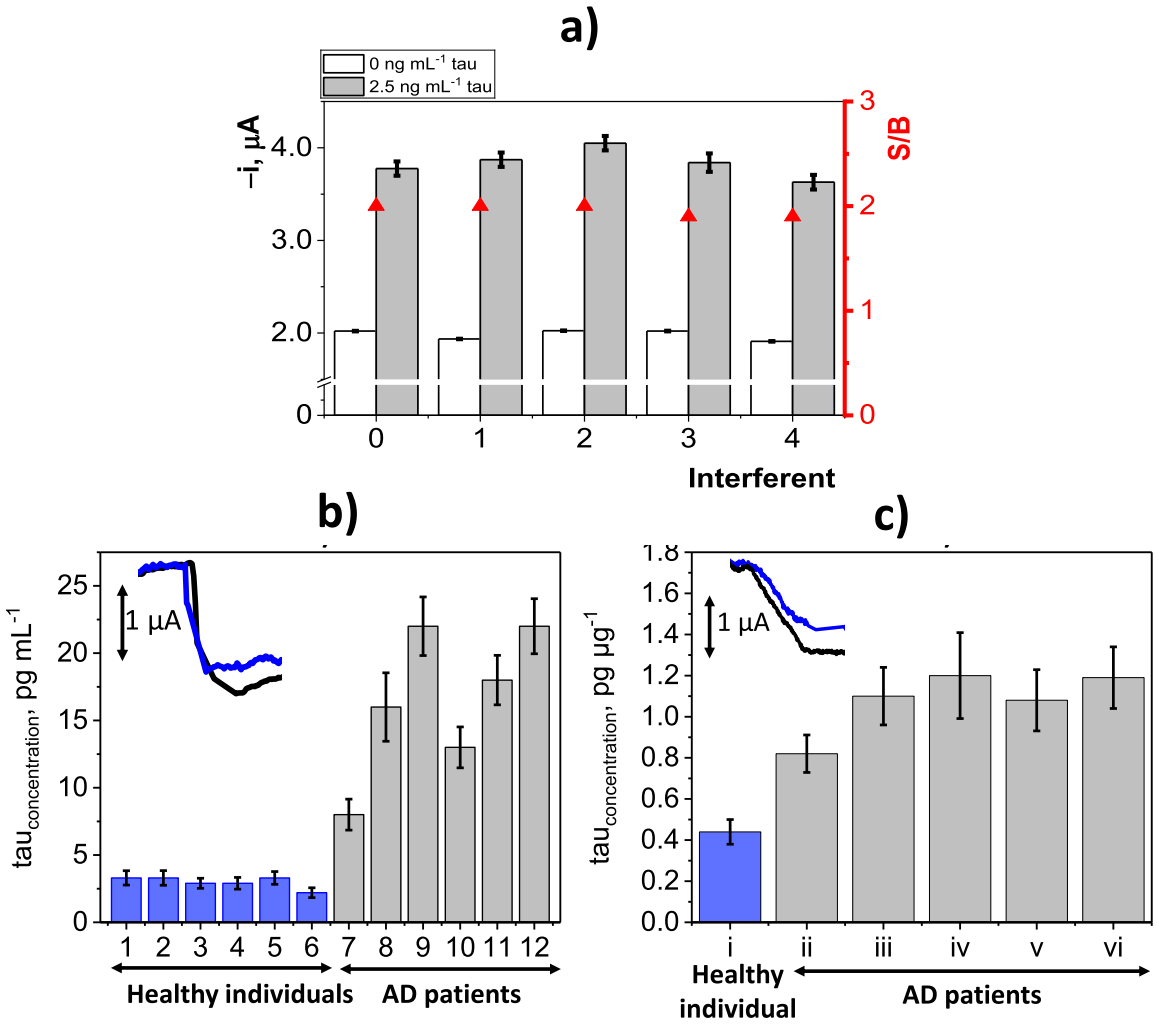

Fig. 4. Amperometric signals measured for 0.0 (white bars) and 2.5 (grey bars) ng mL^{-1} tau standards (and the corresponding S/B ratios, red triangles) prepared in the absence (0) and in the presence of: 1.0 mg mL^{-1} human IgG (1), 5.0 mg mL^{-1} hemoglobin (2), 5.0 mg mL^{-1} BSA (3), 5 mg mL^{-1} HSA (4) a). Amperometric responses measured with the developed immunosensor for the direct determination of tau protein in: b) undiluted plasma samples (5 µL) of healthy individuals (1–6) and *post mortem* diagnosed AD patients (7–12); c) brain tissue extracts (2.5 µg) from a healthy individual (i) and patients diagnosed with AD (ii-vi). Insets: recorded amperograms for a representative healthy individual (blue line) and AD patient (black line). (For interpretation of the references to colour in this figure legend, the reader is referred to the Web version of this article.)

calibration plot constructed with tau standards ((776 ± 36) nA mL ng^{-1}, Fig. 3) and the slope values of the calibration graphs constructed in the spiked representative plasma ($t_{exp} = 8 > t_{tab} = 3.35$) and brain tissue extract samples ($t_{exp} = 3.6 > t_{tab} = 3.35$). Therefore, the determination of the target protein in both kinds of samples was performed using the standard additions method in the presence 2.5 µg of tissue extracts or 5 µL of undiluted plasma samples spiked with increasing concentrations of tau standard solutions (11–800 pg mL^{-1}). Fig. 4b and c shows as tau levels were significantly higher in samples from AD patients than in samples from healthy individuals, in agreement with that reported in the literature (Shui et al., 2018b; Müller et al., 2017). Detailed results are summarized in Table 2.

It is worth remarking that the ELISA methodology using the same immunoreagents is not sensitive enough to determine tau protein in the targeted samples (LODs claimed for the ELISA kits range from 10 to 100 pg mL^{-1} and the clinical cut-off value established in plasma for AD patients is 5 pg mL^{-1}). Therefore, the accuracy of the developed biosensor was tested by analyzing spiked representative plasma and brain tissue protein extracts samples. The results, obtained by applying the same methodology as used for the determination of the endogenous tau content, are summarized in Table S2 in the Supporting Information. As can be deduced, acceptable recoveries were achieved. It is worth noting that the electrochemical immunosensor developed in this work is the first biosensor used for the determination of tau protein in plasma and brain tissue extracts from patients diagnosed with AD.

4. Conclusions

A disposable amperometric immunosensor for the sensitive determination of tau protein, a great relevance AD biomarker, was prepared by implementing a sandwich immunoassay onto SPCEs grafted with *p*-ABA, modified with a 3D-Au-PAMAM nanocomposite and involving an HRP-labeled detector antibody. The immunosensor achieves a LOD value of 1.7 pg mL^{-1}, lower than the clinical cut-off value established in plasma (5 pg mL^{-1}) for AD patients, and has demonstrated pioneering usefulness for the direct determination of tau protein in undiluted human plasma and brain tissue extracts. The immunoplatform is able to provide quantitative results in these complex samples using only 5 µL of plasma or 2.5 µg of tissue extract per determination and involving only a 1 h single incubation step. The great analytical performance exhibited

Table 2
Determination of the endogenous tau protein content in plasma and brain tissue protein extracts from healthy individuals and AD patients.

Samples			[tau], pg mL^{-1}[a]	[tau], ng mg^{-1}[a]	$RSD_{n=3}$, %
Plasma	Healthy individuals	1	3.3 ± 0.3	–	5.4
		2	3.3 ± 0.9	–	5.5
		3	2.9 ± 0.2	–	4.3
		4	2.9 ± 0.3	–	5.0
		5	3.3 ± 0.3	–	4.8
		6	3.3 ± 0.2	–	5.5
	AD patients	7	18 ± 2	–	4.8
		8	16 ± 1	–	5.3
		9	22 ± 1	–	3.3
		10	22 ± 1	–	3.9
		11	22 ± 1	–	3.4
		12	22 ± 1	–	3.1
Brain tissue protein extracts	Healthy individual	i	220 ± 24	0.41 ± 0.05	5.0
	AD patients	ii	413 ± 15	0.83 ± 0.03	3.7
		iii	546 ± 33	1.1 ± 0.1	4.3
		iv	593 ± 37	1.2 ± 0.1	5.8
		v	540 ± 27	1.08 ± 0.05	4.6
		vi	592 ± 25	1.19 ± 0.05	4.2

[a] Mean values ± $ts/\sqrt{n}$; n = 3; α = 0.05.

by the disposable immunosensor and its simple operation with no need for signal amplification strategies, make the developed method an attractive alternative to current methods to identify AD progression in a point of care setting. The proposed amperometric immunoplatform is also competitive with other affinity electrochemical biosensors described so far for tau determination in terms of simplicity, test time, and sensitivity. Despite the promising features demonstrated by the developed methodology, key aspects to focus future efforts include a more exhaustive validation with a larger number of samples and of different nature, the simplification of the working protocol to facilitate its use outside the research laboratory, as well as the performance comparison with new high sensitive methodologies such as Simoa HD-1 protein counting system from Quanterix. In addition, the integration of the developed methodology in multiplexing platforms allowing the simultaneous determination of different biomarkers to increase the diagnostic ability is another important factor to be faced up.

Declaration of competing interest

The authors declare that they have no known competing financial interests or personal relationships that could have appeared to influence the work reported in this paper.

CRediT authorship contribution statement

Claudia A. Razzino: Conceptualization, Investigation, Writing - review & editing, Writing - original draft, Funding acquisition. **Verónica Serafín:** Conceptualization, Investigation, Writing - review & editing, Writing - original draft. **Maria Gamella:** Conceptualization, Investigation, Writing - review & editing, Writing - original draft. **María Pedrero:** Supervision, Writing - review & editing, Writing - original draft. **Ana Montero-Calle:** Investigation. **Rodrigo Barderas:** Supervision, Writing - review & editing, Writing - original draft, Funding acquisition. **Miguel Calero:** Supervision, Writing - review & editing, Writing - original draft. **Anderson O. Lobo:** Writing - review & editing, Writing - original draft. **Paloma Yáñez-Sedeño:** Supervision, Writing - review & editing, Writing - original draft, Funding acquisition. **Susana Campuzano:** Conceptualization, Supervision, Writing - review & editing, Writing - original draft, Funding acquisition. **José M. Pingarrón:** Writing - review & editing, Writing - original draft, Funding acquisition.

Acknowledgements

The financial support of the CTQ2015-64402-C2-1-R (Spanish Ministerio de Economía y Competitividad) and RTI2018-096135-B-I00 (Ministerio de Ciencia, Innovación y Universidades) Research Projects and the TRANSNANOAVANSENS-CM Program from the Comunidad de Madrid (Grant S2018/NMT-4349) are gratefully acknowledged. C.A.R. thanks FAPESP (Grant # 2018/14130-7, Sao Paulo Research Foundation (FAPESP)) for the support granted. R.B. acknowledges the financial support of the PI17CIII/00045 grant from the AES-ISCIII program. A.M-C. was supported by a predoctoral contract of the Fundación Tatiana Perez de Guzman el Bueno and now by a FPU predoctoral contract supported by the Spanish Ministerio de Educación, Cultura y Deporte.

Appendix A. Supplementary data

Supplementary data to this article can be found online at https://doi.org/10.1016/j.bios.2020.112238.

References

An, Y., Jiang, X., Bi, W., Chen, H., Jin, L., Zhang, S., Wang, C., Zhang, W., 2012. Biosens. Bioelectron. 32, 224–230.
Armbruster, D.A., Pry, T., 2008. Clin. Biochem. Rev. 29 (Suppl. i), S49–S52.
Barthelemy, N.R., Fenaill, F., Hirtz, C., Sergeant, N., Schraen-Maschke, S., Vialaret, J., Buee, L., Gabelle, A., Junot, C., Lehmann, S., Becher, F., 2016. J. Proteome Res. 15, 667–676.
Blennow, K., Zetterberg, H., 2015. Nat. Med. 21, 217–219.
Budde, B., Schartner, J., Tönges, L., Kötting, C., Nabers, A., Gerwert, K., 2019. ACS Sens. 4, 1851–1856.
Camacho, C., Matías, J.C., Chico, B., Cao, R., Gómez, L., Simpson, B.K., Villalonga, R., 2007. Electroanalysis 19, 2538–2542.
Camarada, M.B., 2017. J. Phys. Chem. A 121, 8124–8135.
Carlin, N., Martic-Milne, S., 2018. ECS 165, G3018–G3025.
Chiu, M.J., Yang, S.Y., Horng, H.E., Yang, C.C., Chen, T.F., Chieh, J.J., Chen, H.H., Chen, T.C., Ho, C.S., Chang, S.F., Liu, H.C., Hong, C.Y., Yang, H.C., 2013. ACS Chem. Neurosci. 4, 1530–1536.
Conzuelo, F., Campuzano, S., Gamella, M., Pinacho, D.G., Reviejo, A.J., Marco, M.P., Pingarrón, J.M., 2013. Biosens. Bioelectron. 50, 100–105.
Conzuelo, F., Gamella, M., Campuzano, S., Pinacho, D.G., Reviejo, A.J., Marco, M.P., Pingarrón, J.M., 2012. Biosens. Bioelectron. 36, 81–88.
Cook, C.N., Murray, M.E., Petrucelli, L., 2015. Nat. Med. 21, 219–220.
Dai, Y., Molazemhosseini, A., Liu, C.C., 2017. Biosensors 7, 10. https://doi.org/10.3390/bios7010010.
Derkus, B., Bozkurt, P.A., Tulu, M., Emregul, K.C., Yucesan, C., Emregul, E., 2017. Biosens. Bioelectron. 89, 781–788.
Derkus, B., Ozkan, M., Emregul, K.C., Emregul, E., 2016. RCS Adv. 6, 281–289.
Emmrich, E., Franzka, S., Schmid, G., Majoral, J.P., 2002. Nano Lett. 2, 1239–1242.
Esteves-Villanueva, J.O., Trzeciakiewicz, H., Martic, S., 2014. Analyst 139, 2823–2831.
Ferrari, C., Nacmias, B., Sorbi, S., 2018. Neurol. Sci. 39, 615–627.
Gamella, M., Campuzano, S., Conzuelo, F., Reviejo, A.J., Pingarrón, J.M., 2012. Electroanalysis 24, 2235–2243.
Grigorieva, D.V., Gorudko, I.V., Sokolov, A.V., Kosmachevskaya, O.V., Topunov, A.F., Buko, I.V., Konstantinova, E.E., Cherenkevich, S.N., Panasenko, O.M., 2013. Bull. Exp. Biol. Med. 155, 118–121.
Grillo, R., Rosa, A.H., Fraceto, L.F., 2015. Chemosphere 119, 608–619.
Hardy, J.A., Higgins, G.A., 1992. Science 256, 184–185.
Hassan, Q., Kerman, K., 2019. Curr. Opin. Electrochem. 14, 89–95.
Holzinger, M., Goff, A.L., Cosnier, S., 2014. Front. Chem. (Cleveland) 2, 63. https://doi.org/10.3389/fchem.2014.00063.
Jack Jr., C.R., Holtzman, D.M., 2013. Neuron 80, 1347–1358.
Kang, J.H., Vanderstichele, H., Trojanowski, J.Q., Shaw, L.M., 2012. Methods 56, 484–493.
Kim, S., Wark, A.W., Lee, H.J., 2016. J. Anal. Chem. 88, 7793–7799.
Lasagna-Reeves, C.A., Castillo-Carranza, D.L., Sengupta, U., Clos, A.L., Jackson, G.R., Kaye, R., 2011. Mol. Neurodegener. 6, 39. https://doi.org/10.1186/1750-1326-6-39.
Laske, C., Sohrabi, H.R., Frost, S.M., Lopez-de-Ipiña, K., Garrard, P., Buscema, M., Dauwels, J., Soekadar, S.R., Mueller, S., Linnemann, C., Bridenbaugh, S.A., Kanagasingam, Y., Martins, R.N., O'Bryant, S.E., 2015. Alzheimer's Dementia 11, 56–578.
Liu, C.C., Kanekiyo, T., Xu, H., Bu, G., 2013. Nat. Rev. Neurol. 9, 106–118.
Liu, Y., Qing, H., Deng, Y., 2014. Int. J. Mol. Sci. 15, 7865–7882.
Moreno-Guzmán, M., Ojeda, I., Villalonga, R., González-Cortés, A., Yáñez-Sedeño, P., Pingarrón, J.M., 2012. Biosens. Bioelectron. 35, 82–86.
Müller, S., Preische, O., Göpfert, J.C., Carcamo Yañez, V.A., Joos, T.O., Boecker, H., Düzel, E., Falkai, P., Priller, J., Buerger, K., Catak, C., Janowitz, D., Heneka, M.T., Brosseron, F., Nestor, P., Peters, O., Menne, F., Schipke, C.G., Schneider, A., Spottke, A., Fließbach, K., Kilimann, I., Teipel, S., Wagner, M., Wiltfang, J.,

Jessen, F., Lask, C., 2017. Sci. Rep. 7, 9529. https://doi.org/10.1038/s41598-017-08779-0.
Murphy, M.P., LeVine, H., 2010. J. Alzheimers Dis. 19, 311–323.
Nabers, A., Hafermann, H., Wiltfang, J., Gerwert, K., 2019. Alzheimers Dement. (Amst.) 11, 257–263.
Niu, X., Huang, L., Zhao, J., Yin, M., Luo, D., Yang, Y., 2016. Anal. Methods 8, 1091–1095.
Olsson, A., Vanderstichele, H., Andreasen, N., De Meyer, G., Wallin, A., Holmberg, B., Rosengren, L., Vanmechelen, E., Blennow, K., 2005. Clin. Chem. 51, 336–345.
Pei, X., Xu, Z., Zhang, J., Liu, Z., Tian, J., 2013. Anal. Methods 5, 3235–3241.
Roduner, E., 2006. Chem. Soc. Rev. 35, 583–592.
Sánchez, A., Villalonga, A., Martínez-García, G., Parrado, C., Villalonga, R., 2019. Nanomaterials 9, 1745. https://doi.org/10.3390/nano9121745.
Sauter, C., Emin, M.A., Schuchmann, H.P., Tavman, S., 2008. Ultrason. Sonochem. 15, 517–523.
Scarano, S., Lisi, S., Ravelet, C., Peyrin, E., Minunni, M., 2016. Anal. Chim. Acta 940, 21–37.
Serafín, V., Torrente-Rodríguez, R.M., Batlle, M., García de Frutos, P., Campuzano, S., Yáñez-Sedeño, P., Pingarrón, J.M., 2017. Sensor. Actuator. B Chem. 240, 1251–1256.
Serafín, V., Torrente-Rodriguez, R.M., Gonzalez-Cortés, A., García de Frutos, P., Sabaté, M., Campuzano, S., Yañez-Sedeño, P., Pingarrón, J.M., 2018. Talanta 179, 131–138.
Sergeant, N., Bretteville, A., Hamdane, M., Caillet-Boudin, M.L., Grognet, P., Bombois, S., Blum, D., Delacourte, A., Pasquier, F., Vanmechelen, E., Schraen-Maschke, S., Buee, L., 2008. Expert Rev. Proteomics 5, 207–224.
Shui, B., Tao, D., Cheng, J., Mei, Y., Jaffrezic-Renault, N., Guo, Z., 2018a. Analyst 143, 3549–3554.
Shui, B., Tao, D., Florea, A., Cheng, J., Zhao, Q., Gu, Y., Li, W., Jaffrezi-Renault, N., Mei, Y., Guo, Z., 2018b. Biochimie 147, 13–24.
Singal, S., Srivastava, A.K., Kotnala, R.K., Rajesh, 2018. J. Solid State Electrochem. 22, 2649–2657.
Sparks, D.L., Kryscio, R.J., Sabbagh, M.N., Ziolkowski, C., Lin, Y., Sparks, L.M., Liebsack, C., Johnson-Traver, S., 2012. Am. J. Neurodegener. Dis. 1, 99–106.
Tao, D., Shui, B., Gu, Y., Cheng, J., Zhang, W., Jaffrezic-Renault, N., Song, S., Guo, Z., 2019. Biosensors 9, 84. https://doi.org/10.3390/bios9030084.
Tolnay, M., Probst, A., 1999. Neuropathol. Appl. Neurobiol. 25, 171–187.
Vestergaard, M.D., Kerman, K., Kim, D.K., Hiep, H.M., Tamiya, E., 2008. Talanta 74, 1038–1042.
Wang, L.S., Leung, Y.Y., Chang, S.-K., Leight, S., Knapik-Czajka, M., Baek, Y., Shaw, L.M., Lee, V.M.-Y., Trojanowski, J.Q., Clark, C.M., 2012. J. Alzheimers Dis. 31, 439–445.
Wang, S.X., Acha, D., Shah, A.J., Hills, F., Roitt, I., Demosthenous, A., Bayford, R.H., 2017. Biosens. Bioelectron. 92, 482–488.
World Alzheimer Report 2015, 2015. Alzheimer's disease international (ADI), London. https://www.alz.co.uk/research/WorldAlzheimerReport2015.pdf.
Xi, D., Dong, S., Meng, X., Lu, Q., Meng, L., Ye, J., 2012. RSC Adv. 2, 12515–12524.
Yang, S.Y., Chiu, M.J., Chen, T.F., Horng, H.E., 2017. Neurol. Ther. 6 (Suppl. 1), S37–S56.
Zhang, X.A., Shen, J.Z., Ma, H.L., Jiang, Y.X., Huang, C.Y., Han, E., Yao, B.S., He, Y.Y., 2016. Biosens. Bioelectron. 80, 666–673.